Research on Engineering Structures & Materials
www.jresm.org
Research Group

Research Article

A factorial analysis of material composition and operating parameters on tribological properties in graphite-plugged bronze bushings

Amir Alsammarraie [a], Maki H. Zaidan [b], Ali K. A. Aljboury [*,c]

Department of Mechanical Engineering/ College of Engineering/ Tikrit University, Tikrit, Iraq

Article Info

Article History:

Received 22 Dec 2025

Accepted 04 Apr 2026

Keywords:

Self-lubricating bearings;
Factorial design;
effect size;
Multi-objective optimization;
Transient tribology

Abstract

This study investigates the tribological performance of self-lubricating bronze bushings (CuAl10Fe5Ni5) with graphite plugs using a 3^5 full factorial design (243 conditions). Effects of graphite content (10-30%), plug diameter (8-12 mm), applied load (50-150 kg; 0.61-1.84 MPa), sliding speed (250-750 rpm), and sliding time (10-30 min) on coefficient of friction (COF), wear loss, and temperature were quantified. ANOVA with effect size analysis (η^2p) reveals each response is dominated by a distinct factor: applied load controls COF (η^2p = 0.947, 54.65% contribution); graphite content controls temperature (η^2p = 0.696, 44.0%); and sliding speed controls wear loss (η^2p = 0.838, 45.53%). Plug diameter exhibits negligible practical significance ($\eta^2p \leq 0.038$, ≤ 0.62% contribution) despite marginal statistical significance for wear (p = 0.010), establishing substantial design freedom. Increasing graphite content to 30% reduces COF by 29% and wear loss by 58%. Higher loads (150 kg) reduce COF by 54% but increase wear by 59%, revealing a critical multi-objective trade-off. Increasing the sliding speed from 250 to 750 rpm causes thermal degradation (ΔT = 42.6°C), which increases wear loss by 357%. Optimal transient performance—30% graphite, 150 kg (1.84 MPa), 250 rpm—yields COF = 0.150-0.170 and wear loss < 0.100 g. Crucially, steady-state friction was not attained within 2826 m; all values represent running-in behavior. These findings provide quantitative, response-specific design guidelines enabling engineers to prioritize competing performance objectives.

1. Introduction

Tribology is the study of friction, wear, and lubrication, serving as the foundation for the design and longevity of mechanical systems. Bushings, being important parts of rotating machinery, operate under continuous contact and relative movement, and therefore, the aspect of the surface determines the overall reliability and efficiency of the system. In traditional uses, the liquid lubricants, such as mineral oils and greases, offer sufficient protection for the boundary films under moderate operating conditions, but harsh operational conditions, such as very high or very low temperatures, corrosive atmospheres, exposure to radiation, extreme contact pressures, vacuums, or places that cannot be accessed, create extreme conditions whereby traditional liquid lubrication becomes ineffective or impossible [1]. In these conditions, the use of solid lubricants is the only possible method to reduce friction and wear and preserve mechanical performance. Self-lubricating bronze bushings incorporating graphite plugs have found wide application in industry in the fields of aerospace, maritime, high-speed rail, and heavy machinery. These composite materials combine the strong mechanical properties of copper-based alloys, namely strength, durability, and weight-carrying capacity, with the self-lubricating property of graphite. The role of the added graphite is to act as a solid lubricant, which undergoes gradual transfer to the contact

*Corresponding author: eng.alikhalaf1982@gmail.com
[a]orcid.org/0000-0001-7934-1454; [b]orcid.org/0000-0002-6067-4950; [c]orcid.org/0009-0004-3100-3439
DOI: http://dx.doi.org/10.17515/resm2026-1428ma1222rs

surface during the sliding process. This process promotes the formation of a protective layer of transferred material, thus reducing friction and wear to a significant extent. The formed self-replenishing lubrication system eliminates the need for an external lubricant, thus saving maintenance and providing reliable protection in inaccessible locations. Despite strong industrial applications, the complex interrelations of composition, geometric variables, and operational conditions, particularly their combined effect, remain insufficiently established by tribological literature. Most previous studies center around the investigation of single variables, or the joint effect of only one or two variables is considered, and the studies are not comprehensive enough. There are also some geometric uncertainties, especially concerning the diameter of the graphite plug. Common engineering experience is that larger plugs are better from the viewpoint of lubrication, but there is no experimental evidence either supporting or rejecting this hypothesis. In fact, it is quite common in tribology that solid lubricant contacts display nonintuitive behavior under different loading conditions. Classical tribology, which was almost exclusively concerned with lubricated contacts, argues that higher loadings increase contact stresses and thus facilitate wear. Conversely, it has been found in some instances that graphite-filled materials display improved tribological behavior under higher pressure. This is because higher contact pressures are favorable for film formation due to an increasing pressure difference at the interface, thus favoring the extrusion of lubricant material from the matrix into the contact zone. Studies show that the inclusion of graphite significantly reduces both the friction coefficient and wear rate in copper-based bearing materials compared to ordinary copper alloys [1, 2]. For instance, CuSn11 bronze plain bearings impregnated with graphite-filled polytetrafluoroethylene (PTFE) demonstrated reduced friction coefficients and wear loss [3]. CuZn25Al6 bronze with graphite beds was found to have lower values of friction coefficient when the load is constant compared to when it is varied. Copper-graphite composites have, however, been observed to have a critical speed where there is a transition in the friction phenomenon [4]. Different bronze matrices show varied responses to graphite inclusion [1, 2]. Tin bronze-based inlaid solid self-lubricating bearing (ISSLB) materials are always more wear-resistant compared with aluminum bronze-based ISSLB materials, particularly at high loading conditions. Graphite content in the composite has considerable bearing on the performance. In the case of the PTFE-graphite-impregnated bronze specimen with 20 wt % of graphite content, the lowest value of the friction coefficient was observed for the least value of the sliding distance and the highest value of the load. For the specimen with 10 wt% of the graphite content, the best performance resulted for the higher values of the sliding distances and the loads [3]. Self-lubricating bushings, including graphite-plug bushings, can match the performance of, or better that of, conventionally oil- or grease-lubricated bronze bushings (such as high-leaded tin bronze and alloy designation UNS-No. 93200) [5]. Examples of these are the Oiles JM3 and JM7, bronze bearings with graphite and lead plug lubrication. This research identifies the different friction and linear wear values of the several types of bearings, including the aforementioned and others like Thordon, Orkot, DEVA BM, and PAN SoBz, depending on the motion patterns. For instance, the data showed that the Thordon bearings were stable with only slight variations in friction and wear. The experiments on the effects of solid lubricants have shown that the more graphite added, the better the friction and the wear resistance. But there exists no systematic factor analysis of graphite content and parameters of operation, including load and sliding speed. Most past research has focused on single-parameter and two-parameter combinations, highlighting the need for a comprehensive study to examine the complex interactions and optimize the parameter settings. The present study addresses these knowledge gaps by utilizing a comprehensive factor design that includes 243 sets of conditions and 2430 data points. There were five independent variables that were adjusted at three levels, and this allowed the study of effects and interactions of different complexity to establish the best settings of the variables. Factor design also allows the mathematical determination of statistical relationships between composition and operating conditions and tribological properties to give engineering guidance in the design of graphite-filled bronze bushing systems. The influence of the graphite plug diameter on the friction behavior of the graphite-filled bronze bushings was also explored under a broad factor experimental design. Other studies have discussed the overall frictional properties of the graphite alloys of bronze as well as the influence of the graphite content, load, and velocity on the friction and wear but have not done the multivariate analysis to establish the statistical significance of the geometric dimension of the

graphite plugs. This observation is crucial, as it allows for greater flexibility in component design, enabling companies to select plug size based on factors other than frictional capacity, such as price or ease of manufacturing, without compromising the bushing's frictional and wear characteristics.

2. Experimental Details

2.1 Materials

Test samples were made of cylindrical bearing bushings made of copper-nickel aluminum bronze matrix (CuAl10Fe5Ni5) with embedded graphite cylindrical plugs that were placed in the bearing perpendicular to the direction of sliding. These bushings were purchased from Jiashan PVB Sliding Bearing Co., Ltd., China. Table 1 shows the chemical composition of this bronze, according to the product quality certificate issued by the Chinese company (Zhejiang Haima Transmission Technology Co., Ltd.). The hardness of nickel-aluminum bronze is 207 HB. Table 1 presents the parameters of the bushings tested in this work.

Table 1. Chemical composition of bronze (wt%) of CuAl10Fe5Ni5 bronze alloy

Inspection Item	Cu	Al	Fe	Ni	Mn	Zn	Pb	Sn	Si	P
Average	79.882	9.22	5.14	4.76	0.99	0.01	0	0	0	-

The actual bushings are shown in Figure 1. The surface finish (Ra) is consistently between 0.4 and 0.5 μm across all bushings. Three graphite content percentages were tested by one using 10, 20%, and 30% by coverage. The content variation was done by changing the quantity and distance between cylindrical plug inserts of graphite in the bronze matrix when they were being manufactured. Three graphite plugs were tested: 8 mm, 10 mm, and 12 mm. Each of the specimens was machined to typical dimensions of bearing geometry (length 20 mm, bore diameter 40 mm, and outer diameter 50 mm) (typical of industrial bearing use). The shaft material is made of hardened AISI 410 steel, which has a modulus of elasticity of 200 GPa and a hardness of 230 ± 10 HB and a diameter of 40 mm. Applied loads were applied as dead weights of 50 kg, 100 kg, and 150 kg, which correspond to a normal force of 490.5 N, 981.0 N, and 1,471.5 N, respectively. The chemical composition of the shaft is [Fe-(0.12) C-(0.9) Mn-(0.8) Si-(0.68) Ni-(12.5) Cr-(0.03) P-(0.02) S wt.%]. This metal is characterized by high strength and hardness, and it contains a high percentage of carbon, which makes it excellent for corrosion resistance. As a result, 410 steel is appropriate as the opposing grinding component to evaluate the friction performance of copper alloys.

Fig. 1. Bushing from nickel-aluminum bronze with graphite plugs

2.1.1 Contact Pressure Calculation

For cylindrical journal bearing geometry (bushing bore diameter = 40 mm, length = 20 mm), the nominal projected contact pressure was calculated to provide engineering-relevant stress values. The calculation uses the normal force derived from the applied dead weights and the projected contact area of the bushing. The nominal projected contact pressure is calculated as:

$$P = F_N/A = (F_N)/(L \times d) \quad (1)$$

Where P = nominal contact pressure (MPa), F_N = normal force = applied mass (kg) × 9.81 m/s^2, A = projected contact area (mm^2) = bushing length × bore diameter, L = bushing length = 20 mm = 0.020 m, and d = bore diameter = 40 mm = 0.040 m.

2.2 Tribological Testing Apparatus

Tribological testing was conducted on a tribometer that was designed by Tikrit University. The experimental setup is shown in Figure 2. The test bushing sample is mounted as a fixed part, and the shaft of the testing bench is rotated at a specified angular velocity (250, 500, or 750 rpm) about its central axis. The counter-surface (shaft) of a standard 40 mm diameter of steel was kept in rotary contact with the surface of the specimen at a normal force of a predetermined weight load (490.5, 981, or 1471.5 N). A normal force was applied via a manual loading system consisting of a load transfer arm and a load cell (range 0-200 kg), which senses the amount of applied load and converts it into an electrical signal that is transmitted to a digital weighing indicator that converts the electrical signal into digital data that can be manually recorded. The load transducer arm used to apply the load is mounted on the sample housing and is in contact with the load cell. The frictional force during sliding was continuously monitored via a friction load transducer arm mounted in the sample housing that was in contact with a load cell (range 0-25 kg, accuracy ±0.05 kg), with the load cell output converted into digital data that could be read by an indicator and recorded manually. Friction temperature in a sliding contact area was measured using a calibrated K-type thermocouple that has a response speed of less than 100 ms, with data synchronized with friction force measurement. The weights of bushing samples before and after testing were measured using electronic scales with an accuracy of 0.001 g. All experiments were done in a lab environment with normal conditions in terms of temperature of 22-25°C, humidity of 40-60%, and pressure of 101 kPa.

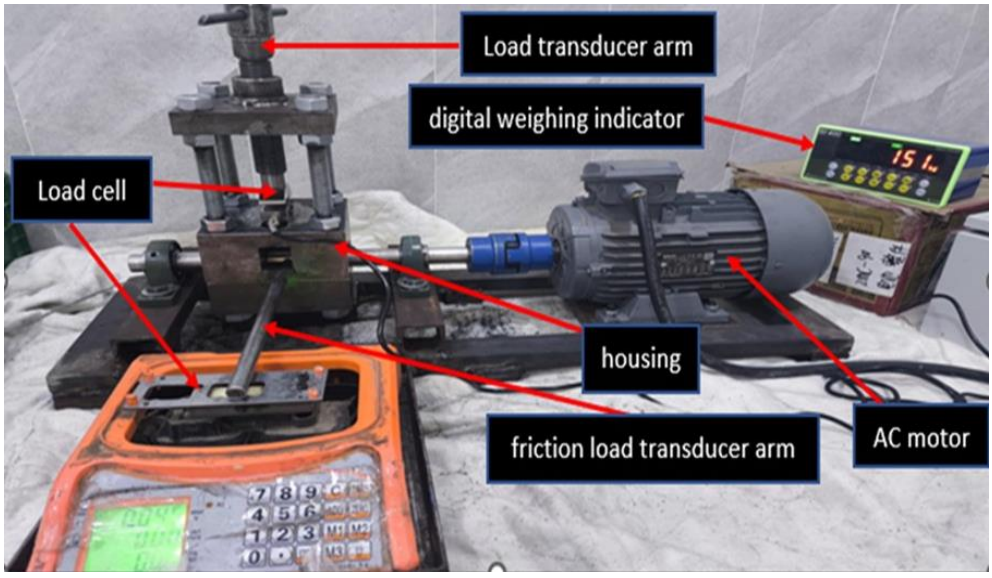

Fig. 2. Experimental setup

2.3 Testing Procedures

Sample pieces were checked to ensure the correct dimensions with the tolerances of ±0.05 mm. To remove machining fluids and contaminants, the test surfaces of the specimens were blotted with ethanol and left to dry before the tests were conducted. The steel shaft was polished with grade 1000 emery paper to maintain the uniform surface roughness of the counter surface during the entire experiment. Roughness of the inner surface of each bushing sample was measured and recorded before and after testing. The electric motor speed is set to the desired speed using a speed controller before starting the test. The test was conducted for a specified duration with constant parameters. The loss was calculated using the following formula:

$$Wear\ loss\ (g)\ =\ (Initial\ mass\ -\ Final\ mass) \tag{2}$$

The sliding distance was calculated as follows:

$$Sliding\ distance\ (m)\ =\ (Speed\ [rpm]\ \times\ 2\pi\ \times\ Radius\ [m]\ \times\ Time\ [min])\ /\ 60 \tag{3}$$

The wear rate, which represents the material loss per unit of sliding distance, was calculated as follows:

$$Wear\ rate\ (g/m)\ =\{Initial\ mass\ (g)\ -\ Final\ mass\ (g)\}\{Sliding\ distance\ (m)\} \tag{4}$$

Sliding distance (D) and sliding time (t) have a determinate relationship in terms of the sliding speed (v), where the relationship is given by D = v * t. In the present investigation, the values of the sliding speeds and the sliding times adopted were 250, 500, and 750 rpm and 10, 20, and 30 min, respectively, resulting in six different values of the sliding distance: 314, 628, 942, 1256, 1884, and 2826 m. This determinate relationship of the variables raises the issue of multicollinearity in factorial experiments when both the variables of time and speed are used as independent variables. To assess multicollinearity, variance inflation factors (VIF) were calculated for all independent variables (Table 2):

Table 2. Variance inflation factor (VIF) analysis

Factor	VIF	Tolerance	Multicollinearity Assessment
Graphite content	1.02	0.980	Negligible
Graphite Plug Diameter	1.01	0.990	Negligible
Sliding Speed	1.87	0.535	Moderate (acceptable)
Applied Load	1.04	0.962	Negligible
Sliding Time	1.91	0.524	Moderate (acceptable)

All the values of VIF remain less than 2.0, which indicates that multicollinearity does not appear to be of a nature that would impact the ANOVA. The moderate correlation between speed and time (r = 0.68) is built into the design but remains within acceptable limits. In calculations related to the effect of distance, distance is considered a derived factor rather than an independent one.

The friction coefficient was estimated using the equations [4]-[8]. The experiments were conducted in dry conditions. The following terms are used in Figure 3: M_O the moment point, M_S the moment generated by friction force, M_L the moment generated by rotation force measured by load cell, F_S the friction force (N), F_L the rotation force measured by load cell during rotation (N), μ the friction coefficient, L the distance between load cell and shaft center (mm), and r_1 the distance between contact point and shaft center (mm). With $\sum M_O = 0$

$$M_S = M_L \tag{5}$$

$$F_S \times r_1 = F_L \times L \tag{6}$$

$$F_S = F_L \times {}^{L}/_{r_1} \tag{7}$$

$$F_S = \mu \times F_N \tag{8}$$

$$\mu = {}^{F_S}/_{F_N} \tag{9}$$

These values represent the nominal projected contact pressure in an ideal conforming contact situation. In practice, the actual contact pressures at asperity junctions are significantly increased due to surface roughness. The range of actual contact pressures, i.e., 0.61 to 1.84 MPa, corresponds to the typical working pressures of graphite-plugged bronze bushings in moderate load-bearing applications [5, 6].

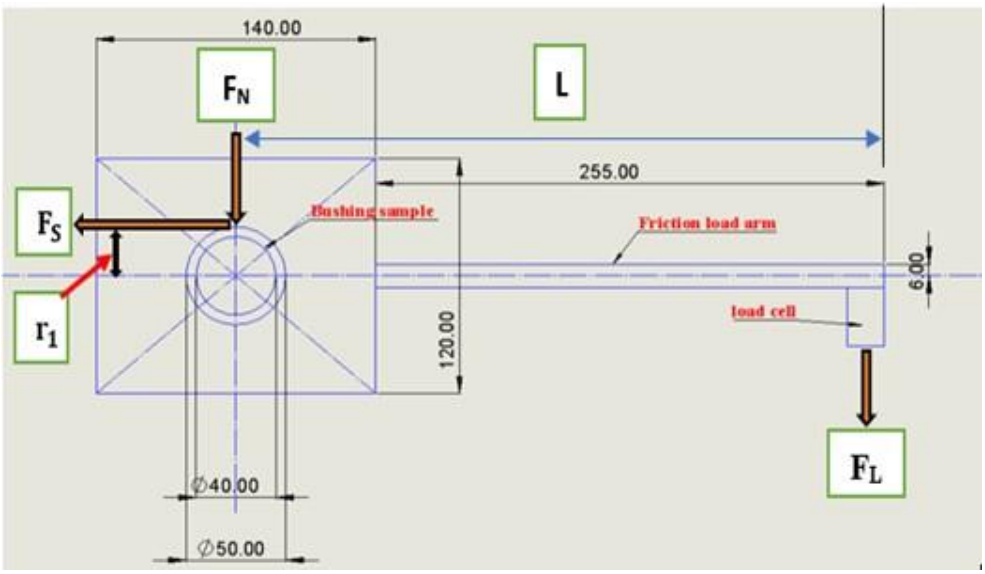

Fig. 3. The bushing wear test mechanism

The linear sliding velocity at the contact interface was calculated from the rotational speed and shaft diameter:

$$v\left(\frac{m}{s}\right) = \frac{\pi \times d \times N}{60} \tag{10}$$

Where, d = shaft diameter, N = rotational speed. This yields the following linear velocities:

- 250 rpm $\rightarrow v = \frac{\pi \times 0.04 \times 250}{60} = 0.524$ m/s
- 500 rpm $\rightarrow v = \frac{\pi \times 0.04 \times 500}{60} = 1.047$ m/s
- 750 rpm $\rightarrow v = \frac{\pi \times 0.04 \times 750}{60} = 1.571$ m/s

2.4 Data Analysis

The study employed a 3^5 full factorial experimental design to analyze five independent variables, which were tested at three distinct levels. The independent variables consisted of graphite content levels at 10%, 20%, and 30%; graphite plug diameter measurements of 8 mm, 10 mm, and 12 mm; sliding speed settings at 250 rpm, 500 rpm, and 750 rpm; applied load values of 490.5 N, 981 N, and 1471.5 N; and sliding time intervals at 10 minutes, 20 minutes, and 30 minutes. The complete factorial design generates 3^5 = 243 distinct experimental combinations. Each combination was tested once (single replicate). The statistical analysis needed to compute the average values and standard deviations together with minimum and maximum values for every dependent variable in all 243 experimental conditions and each independent variable level. Two-way and higher-order ANOVA was performed to test the statistical significance of main effects (each independent variable) and selected two-way interaction effects. The null hypothesis H_0 states that all group means are equal, but the alternative hypothesis H_1 suggests that at least two group means show differences. The test statistic F = (Mean Square Between) / (Mean Square Error) was calculated for each factor. P-values were determined from cumulative F-distribution with appropriate degrees of

freedom. The study established $\alpha = 0.05$ as the significance threshold before analysis, and any factor with $p < 0.05$ was deemed statistically significant.

Each of the experimental combinations was evaluated once; that is, there was a single replicate for each combination. This decision was dictated by the fact that performing a full factorial replication of the experiment would have entailed performing between 486 and 729 individual tests, each of which has its own set of precise and intricate preparation and test protocols. However, the choice also has important implications for the results obtained. Without replication, the mean square error (MSE) for ANOVA is based solely on higher-order interactions and not on pure experimental error. This has the potential to artificially inflate statistical power and result in an increased probability of Type I errors (false positives) [7, 8]. To overcome this limitation of the experimental design, we adopted the following strategies: (1) a conservative approach to interpreting results for which marginal significance was indicated (i.e., p-values between 0.01 and 0.05); (2) the additional use of effect size indices of statistical significance, which are less subject to sample size artifacts than are p-values; (3) a sensitivity analysis in which three-way and higher-order interactions were grouped with error; and (4) validation of key results against physically meaningful thresholds.

Additionally, experimental variability was characterized by:

- Determining the standard deviations for all the calculated mean values
- Determining the 95% confidence interval for all the effect sizes (partial eta squared, $\eta^2 p$)
- Performing Levene's tests for homogeneity of variances (Table 17)
- Performing residual analysis to check the assumptions for ANOVA (Section 4.4, Figure 11)

3. Results and Discussion

3.1 Friction Coefficient

The experimental design includes three graphite content percentages (10%, 20%, 30%) three graphite plug diameters (8 mm, 10 mm, 12 mm), three sliding speeds (250 rpm, 500 rpm, 750 rpm), three applied loads (490.5 N, 981 N, 1471.5 N), and three sliding time intervals, resulting in six main sliding distances (314 m, 628 m, 942 m, 1256 m, 1884 m, 2826 m). Table 3 below shows the values of the coefficient of friction, which is considered the most important independent factor, and includes the average initial and final coefficient of friction and the percentage change in the same factor over the length of the test distance. Figure 4 presents a comprehensive analysis of friction behavior, consolidating the key findings into a single multi-panel figure.

Table 3. Coefficient of friction versus each major sliding distance for all applied loads

Applied Load (kg)	Applied Load (N)	Pressure (MPa)	Initial μ (at 314 m)	Final μ (at 2826m)	Percentage Increase
50	490.5	0.613	0.220	0.433	96.37 %
100	981	1.226	0.141	0.2542	84.1 %
150	1471.5	1.839	0.107	0.2003	86.91 %

The mean coefficient of friction increased continuously by approximately 90% from 314 m to 2826 m (Table 4), without subsequent stabilization or decrease. This monotonic increase throughout the entire test duration indicates that the system operated entirely within a transient running-in regime and did not attain steady-state friction conditions. In accordance with well-established tribological principles, steady-state friction is characterized by a constant mean COF with minor variations around a stable value, indicating equilibrium between film formation and removal. The absence of such stabilization within the 2826 m test duration has three important implications:

- The reported optimal COF values of 0.150-0.170 represent minimum friction achieved during running-in at the shortest sliding distances, not equilibrium coefficients.
- Comparative assessments between factor levels remain valid, as all conditions were evaluated under identical transient protocols.
- Extended testing beyond 2826 m would be required to determine steady-state attainment distances.

Table 4. Average, minimum, and maximum COF values for each key sliding distance

Sliding Distance (m)	Mean COF	Minimum COF	Maximum COF	Number of Data Points
314	0.1562	0.0913	0.2629	27
628	0.1887	0.0883	0.3504	54
942	0.2144	0.0820	0.3744	54
1256	0.2253	0.0966	0.4015	27
1884	0.2615	0.0924	0.4875	54
2826	0.2968	0.0882	0.5666	27

The absence of friction stabilization within the 2826 m test duration necessitates special attention when considering the optimal performance conditions reported. In accordance with well-established tribological principles [9, 10], steady-state friction is characterized by a constant mean coefficient of friction (COF) with minor variations around a stable value, indicating equilibrium between film buildup and film breakdown. In the current study, the continuously increasing COF values over all ranges of sliding distance from 314 m to 2826 m verify that the system remained in Stage I (transient running-in) of the conventional three-stage friction evolution model (Fig. 4 [9]) without entering Stage II (steady-state) or Stage III (lubricant starvation failure).

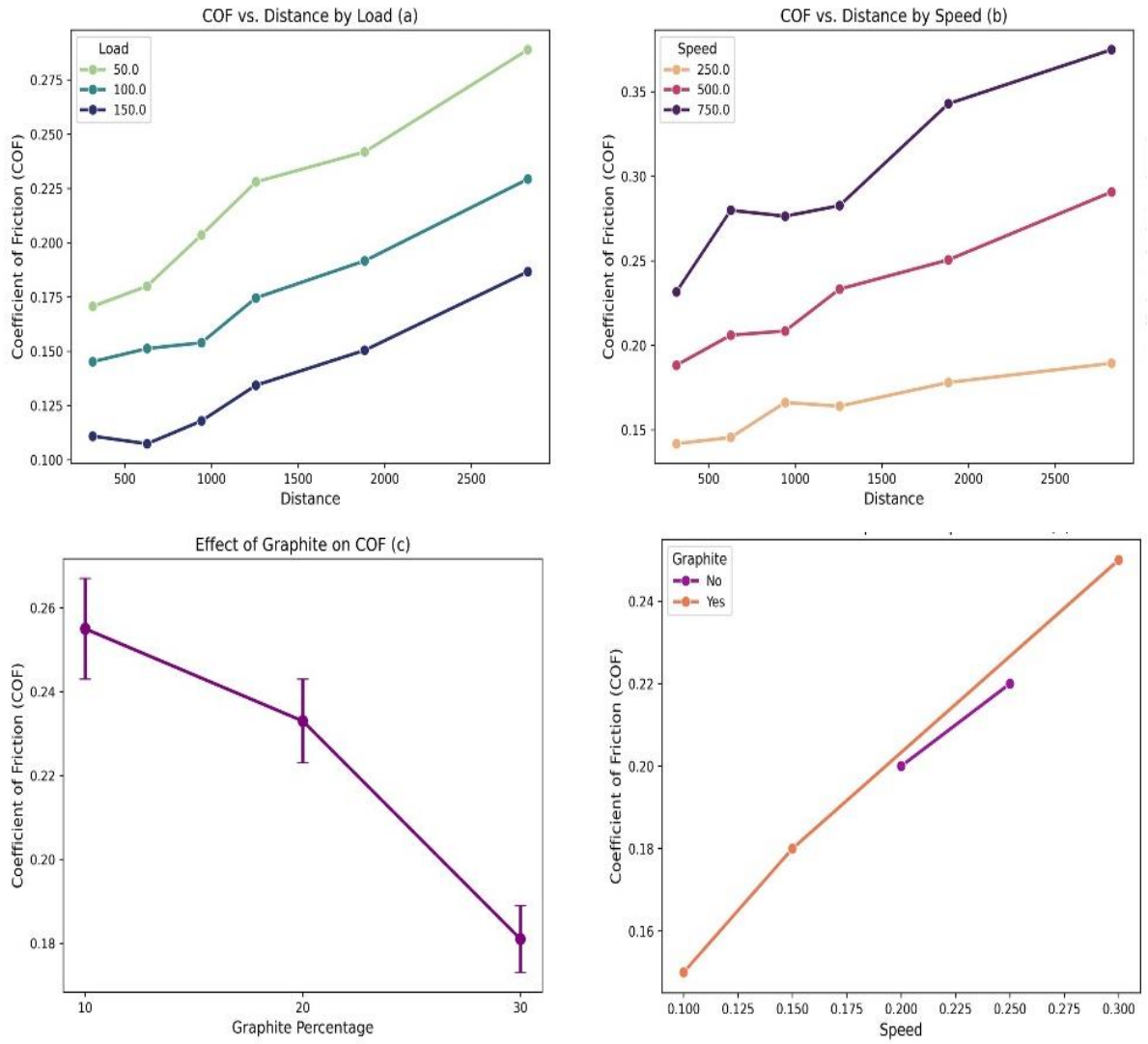

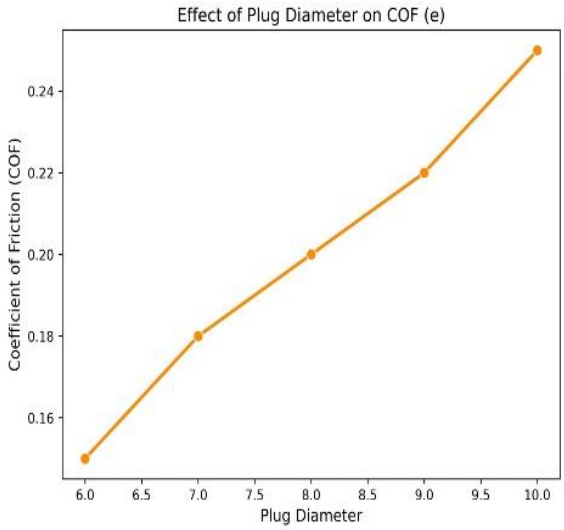

Fig. 4. Comprehensive analysis of friction behavior

This transient running-in state has three important implications for the current study:

- The reported optimal values of 0.150-0.170 were merely indicative of minimum friction values, as experienced during running-in, at the shortest distance ranges, and do not represent equilibrium friction coefficients.
- The 29% improvement in COF due to an increase in graphite content is verified as an accurate comparative analysis, whereas it is assumed that these values would be even lower for all materials under steady-state running conditions.
- Further testing beyond 2826 m would be required to determine if, and at what distance, these graphite-plugged bronze bushings will achieve steady-state friction, as well as determine if the performance ranking of these materials will be maintained under equilibrium running conditions.

Thus, it is submitted that the "optimal tribological performance" reported in this current study should be understood as optimal transient performance, as experienced during running-in, as opposed to optimal steady-state performance. Figure 4(a) illustrates the relationship between COF and sliding distance for the three applied loads. At the lowest load (490.5 N), COF increases gradually from 0.220 at 314 m to 0.433 at 2826 m. Increasing the load to 981 N reduces COF across all distances, with values ranging from 0.141 to 0.254. At the highest load (1471.5 N), COF is further reduced to 0.107-0.200 (Table 3). Aggregating data across all distances reveals a 54.2% reduction in mean COF from 0.3225 at 490.5 N to 0.1479 at 1471.5 N (Table 5). Correlation analysis confirms a strong negative relationship ($r = -0.719$), identifying applied load as the second-most influential factor after graphite content percentage. This inverse relationship is consistent with modern friction theory: increased applied load increases the real contact area while reducing contact stress and simultaneously promotes graphite extrusion and transfer film formation under higher contact pressures [2, 11, 12].

Table 5. Mean, minimum, and maximum values of the COF for each applied load

Applied Load (N)	Average COF (μ)	Minimum COF	Maximum COF	Number of Data Points
490.5	0.3225	0.1983	0.5666	81
981	0.1987	0.1152	0.3511	81
1471.5	0.1479	0.0820	0.2910	81

Figure 4(b) demonstrates the pronounced influence of sliding speed on COF. At 250 rpm, COF remains relatively stable between 0.156 and 0.193 across the sliding distance (Table 6). At 500 rpm, COF increases to 0.199-0.250. At 750 rpm, COF reaches 0.235-0.297. The mean COF increases by 52.3% from 0.176 at 250 rpm to 0.268 at 750 rpm (Table 7). Correlation analysis confirms a

strong positive relationship (r = 0.658). This speed-dependent increase is attributed to frictional heating (temperature elevation from 100.2°C to 142.8°C, Table 8), which degrades graphite's lubricating efficacy through adsorbed water vapor desorption and increased shear stresses at the interface [13–15]. As it is illustrated in Figure 4(b), the best operating conditions are proper at lower speeds (250 rpm) with a short distance of sliding. The mean COF also tends to rise with the severity of the operation (greater speeds and longer distances), implying the lower predictability of tribological behavior. The results of several studies confirm the fact that in the case of bronze bushings with graphite or graphite-filled PTFE, the coefficient of friction (COF) usually rises when the sliding speed is higher under dry conditions. The results of the experiment with bronze and graphite inserts demonstrate a definite tendency: the coefficient of friction rises with the increasing sliding speed [13]. This has been due to the change of the contact interface and heat generation at high speeds that can decrease the performance of solid lubricants such as graphite. Nevertheless, the relationship is not necessarily linear. It has been observed in some studies that at a certain speed or under certain conditions the coefficient of friction can stabilize or even decrease due to a change in the lubrication system or softening of the materials. The use of graphite typically reduces the overall coefficient of friction of unfilled bronze, although a significant increase in the speed-related coefficient of friction remains [14]. Graphite content emerged as the dominant material factor.

Table 6. Mean COF by sliding distance

Sliding Speed (rpm)	Sliding Distance (m)	Mean COF	Min COF	Max COF	Samples
250	314	0.156	0.091	0.263	27
250	628	0.179	0.088	0.326	27
250	942	0.193	0.082	0.335	27
500	628	0.199	0.116	0.350	27
500	1256	0.225	0.097	0.402	27
500	1884	0.250	0.092	0.488	27
750	942	0.235	0.127	0.374	27
750	1884	0.273	0.104	0.481	27
750	2826	0.297	0.088	0.567	27

Table 7. Mean COF by sliding speed

Sliding Speed (rpm)	Linear Velocity (m/s)	Average Coefficient of Friction (COF)
250 rpm	0.524	0.176
500 rpm	1.047	0.225
750 rpm	1.571	0.268

Figure 4(c) shows the effect of graphite content on mean COF. Increasing graphite content percentage from 10% to 30% reduces mean COF from 0.255 to 0.181—a 29.0% reduction (Table 8). The effect size is considerable ($\eta^2 p = 0.760$, $p < 0.001$), indicating that the main material factor is the coverage of graphite. This reduction is significantly better than that achieved in similar systems (35% [1] and 42% [10]), because of the synergetic combination of the high-strength CuAl10Fe5Ni5 bronze matrix and the uniformly distributed plugs of graphite that support the transfer film formation effectively [15].

The interaction between graphite content percentage and sliding speed is shown in Figure 4(d). The parallel nature of the lines shows that there was no significant interaction between these parameters, with the friction reduction effect of graphite content percentage being consistent at all speeds and the friction enhancement effect of increased speed being independent of graphite content.

Table 8. Main effects of material and operating parameters on coefficient of friction

Parameter	Level	Mean COF (μ)	Δ%	95% CI	n	Effect Size (η^2p)
Graphite content	10%	0.255	Baseline	[0.243, 0.267]	81	0.760
	20%	0.233	-8.6%	[0.221, 0.245]	81	(Very Large)
	30%	0.181	-29.0%	[0.172, 0.190]	81	
Plug Diameter	8 mm	0.225	Baseline	[0.214, 0.236]	81	0.010
	10 mm	0.218	-3.1%	[0.207, 0.229]	81	(Negligible)
	12 mm	0.226	+0.4%	[0.215, 0.237]	81	
Sliding Speed	250 rpm	0.176	Baseline	[0.168, 0.184]	81	0.824
	500 rpm	0.225	+27.8%	[0.214, 0.236]	81	(Very Large)
	750 rpm	0.268	+52.3%	[0.257, 0.279]	81	

It can be observed from Figure 4(e) that the diameter of the graphite plug does not significantly affect the coefficient of friction (COF). The average COF values are observed to be 0.225 for a plug diameter of 8 mm, 0.218 for a plug diameter of 10 mm, and 0.226 for a plug diameter of 12 mm, with a maximum difference of only 0.33% (Table 9). Analysis of variance confirms the absence of statistical significance ($p = 0.291$) with a small effect size ($\eta^2p = 0.010$). The finding has important practical implications. The diameter of plugs can be determined based on various factors such as manufacturing efficiency, structural properties, and aesthetics.

Table 9: Mean COF by graphite plug diameter

Graphite Plug Diameter (mm)	Average Coefficient of Friction (COF)
8	0.225
10	0.218
12	0.226

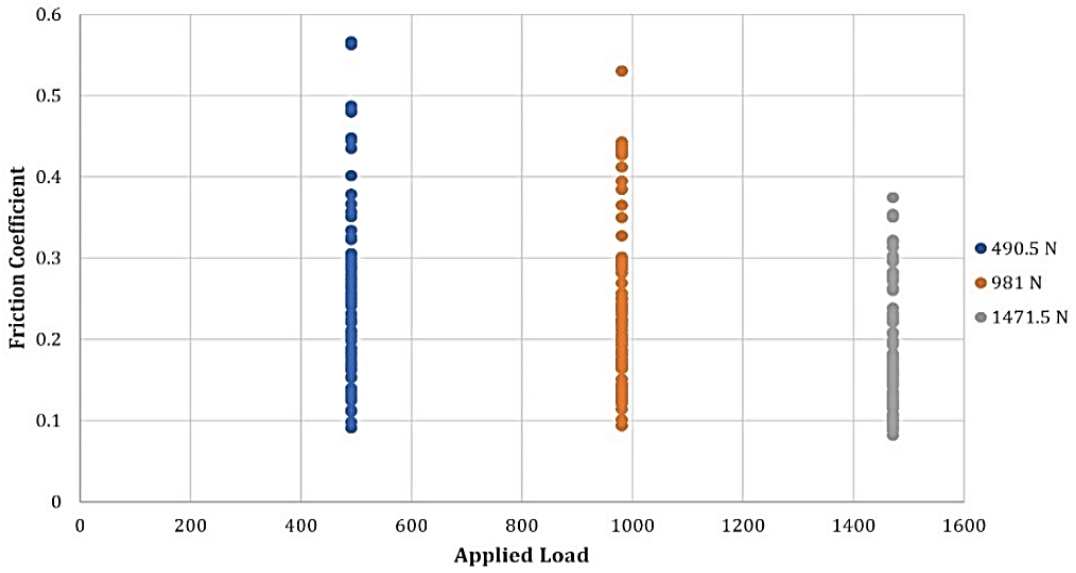

Fig. 5. Applied load vs. coefficient of friction

Figure 5 illustrates the relationship between the coefficient of friction and the applied load. This scatter plot shows the negative correlation between applied load and coefficient of friction, indicating that as applied load increases, which ranges between 490.5 and 1471.5 N, the values of coefficient of friction decrease with the difference in applied load at each of the 243 data points. Aggregating data across load levels yields a convincing numerical representation of this effect. The correlation coefficient ($r = -0.719$) indicates load as the second-most influential factor after

graphite content. The analysis reveals a strong inverse correlation between normal applied load and coefficient of friction. Materials that show better lubrication or surface conformity at higher pressures tend to exhibit this behavior. This behavior is likely related to the load-dependent behavior of graphite. At high contact pressures, the solid lubricant is thought to transfer more efficiently from the solid to the surface of the mating component (where the mating surfaces are in contact). This, in turn, helps to form a better lubricating film and less shear stress between the two components. As a result, there is less contact between the asperities of the two surfaces, thus creating lower overall friction. Several studies indicate that the coefficient of friction (COF) of graphite-filled and graphite-coated bronze liners decreases with increasing (normal) load. The increased formation and stability of the lubricating graphite films under increasing load leads to reduced friction and direct contact between the two metals [3, 11, 16, 17].

3.1.1 Mechanistic Interpretation

Load-Dependent Friction Reduction: The observed reduction in COF with increasing applied load (54.2% from 50-150 kg) requires careful mechanistic interpretation with appropriate acknowledgment of evidentiary limitations. Elevated contact pressure increases the hydrostatic pressure gradient at the graphite-bronze interface, promoting extrusion of solid lubricant from reservoir plugs to the sliding surface [12], [16]. This is supported by:

- Linear correlation ($r = -0.719$) between load and COF.
- Correspondence with published observations in similar material systems [2, 16].
- Physical plausibility based on pressure-driven flow.

There are also possible alternative mechanisms:

- The evolution of the actual contact area under load [13].
- The effects of frictional heating on the orientation of graphite crystals [18].
- Particle fragmentation by a third body and compression of the transport layer [19].

3.1.2 Interaction Effects Analysis

The full factorial design allows for a thorough examination of two-way interactions between factors. Figure 4(d) shows the interaction between graphite content and sliding speed. The parallel nature of the lines shows that the effect of increased graphite content on friction is consistent across all speeds, as is the effect of increased speed on friction, irrespective of graphite content. ANOVA results show no interaction between graphite content and sliding speed, i.e., $p > 0.05$.

Table 10 summarizes all significant two-way interactions. The greater slope of the load-wear curve at higher speeds signifies a synergistic effect, wherein the effect of the load on wear is amplified at higher speeds. This relationship is statistically significant ($p < 0.01$) and has significant implications for the control of wear, wherein the effect of the load becomes more significant as the speed increases. These interactions underscore the need for multi-objective optimization and demonstrate that factor effects cannot be considered in isolation.

Table 10. Significant two-way interactions

Interaction	Response	p-value	Interpretation
Load × Speed	Wear Loss	<0.01	Synergistic - load effect amplifies with speed
Load × Graphite	COF	<0.05	Antagonistic - graphite benefit reduces at high load
Speed × Time	Wear Loss	<0.05	Cumulative - combined effect exceeds sum of individual

3.2 Wear Loss

The wear loss, which is determined as the difference between the weight of the bushing before and after testing (Δm), is the main dependent variable for this study. Wear is greatly influenced by sliding speed, temperature, graphite content percentage, applied load, and sliding distance. Table 11 shows the average, maximum, and minimum wear loss values for each sliding speed based on 243 experimental data points. The average wear loss was 0.099 g at 250 rpm, while it was 0.348 g

at 500 rpm (which is a 252% increase over 250 rpm), and the average wear loss at 750 rpm was 0.449 g (which is a 354% increase over 250 rpm).

Table 11. Summary of wear loss values for each sliding speed

Sliding Speed (rpm)	Linear Velocity (m/s)	Average Wear Loss (g)	Number of Data Points	Min. Wear Loss (g)	Max. Wear Loss (g)
250	0.524	0.0989	81	0.0457	0.1812
500	1.047	0.3482	81	0.0974	0.8390
750	1.571	0.4493	81	0.1424	1.0280

Strong positive correlation with wear loss (r = 0.658) identifies speed as the dominant operational wear driver. Figure 6 illustrates the effect of sliding speed on wear loss. As can be seen from the figure below, the relationship between sliding speed and wear loss is not linear, but a higher rate of increase was observed from 250 to 500 rpm (an increase of 252%) compared to 500 to 750 rpm (an increase of 29%). All these statistical tests indicate significant differences in the rate of increase differences between speed levels. By examining the results, it was observed that the wear loss in graphite-plugged bronze bushings is highly dependent on the sliding speed, showing a non-linear relationship with accelerated wear rates at higher speeds. Numerous experiments conducted on graphite-embedded bronze bushings, as well as on other self-lubricating compounds, have shown that wear loss can be reduced by increasing the sliding speed, especially under dry conditions [3]. The effect of sliding speed on wear is not straight, and it varies with factors like the composition of the materials, the load, and the environmental conditions.

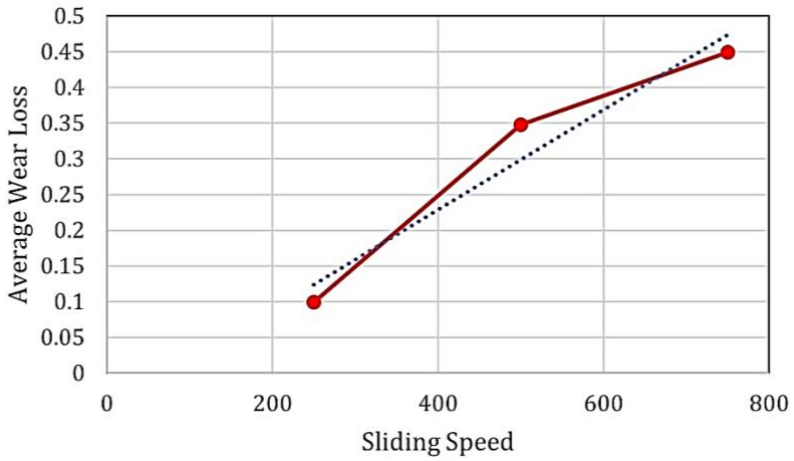

Fig. 6. Effect of sliding speed on wear loss

When the operational speed goes up, the loss of the material increases considerably, which means that there is a strong connection between these parameters for the durability and lifespan of the bushings. Several factors may have contributed to the observed relationship:

- Thermal Effects: The frictional heat generated due to the increased sliding speed is one of the factors that can negatively impact the graphite-bronze interface and solid lubrication. If the flash temperature goes beyond a certain limit (for example, 360 K), the lubricating property of graphite is lost, thus resulting in the switching from solid lubrication to adhesive wear [10, 14].
- Mechanical Stress: The increase in speed causes the shear stresses at the interface to rise, and thus interfacial wear to occur more quickly, especially when loads are higher [6, 15].
- Lubrication Breakdown: The self-lubricating properties of graphite could be lost at high speed, resulting in increased friction and wear. The creation and permanence of a lubricating film are very important; if they are interrupted, the wear rates will increase dramatically [6, 10, 14].

- Surface Roughening: Higher speeds cause rapid surface degradation, which leads to friction and wear increase, while rough surfaces contribute to the abrasion and adhesion wear mechanisms [12, 15].

High temperatures of self-lubricating systems such as graphite-plugged bushings may have an impact on the effectiveness of the solid lubricant film transfer, which may result in more metal-to-metal contact and quicker wear. The statistical analysis of average values at each speed setting provides exact measurements of these trends and shows how strongly they affect the results. Table 11 indicates that the transition from a speed of 250 to 750 rpm leads to an increase in the average temperature by over 42°C. This suggests that temperature is a consequence of the energy input, which is controlled by speed, rather than an independent variable. Figure 7 clearly shows the correlation between temperature and wear loss. Key observations include:

- General trend: As the temperature increases from its lower range, approximately 60-100°C, to the higher range, approximately 160-200°C, the wear loss associated increases from less than 0.1 to over 1.0 g, which is an order of magnitude increase.
- Clustering by speed: The data points are organized into three distinct clusters, which represent the three different sliding speeds, but these clusters show some degree of overlap with each other. The tests carried out at a speed of 250 rpm produce a particular cluster with low temperatures and little wear. The tests conducted at a 750 rpm speed create a single cluster, which shows both high temperature levels and high wear rates. The tests at 500 rpm speed produce results that establish the middle ground between the two other speed settings.
- Mechanism implication: The clustering patterns demonstrate that sliding speed functions as the main experimental factor, which affects both the temperature increase and the wear rate. As speed increases, friction generates more heat, which causes temperatures to rise. The combination of thermal effects and elevated mechanical stress from faster speeds results in an accelerated wear process.

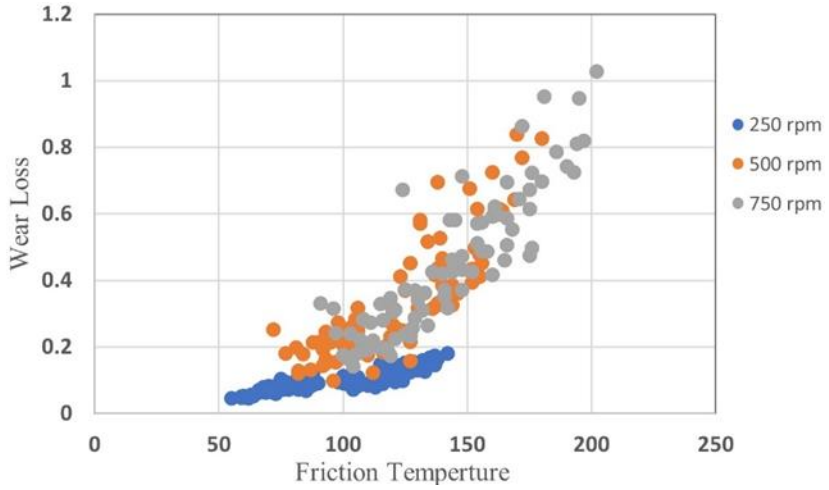

Fig. 7. Scatter plot of wear loss and friction temperature by sliding speed

Temperature rise has a direct impact on material degradation and wear, their rates increasing considerably under demanding operating conditions [14]. Although the lubricating effect of graphite helps in wear reduction, it loses its effectiveness when the temperature and load increase, thus introducing wear at a faster pace [15]. Sliding distance is always designated to be a significant parameter that influences wear loss in graphite-plugged bronze bushings and other self-lubricating composites of this type. By measuring the wear rate (wear loss per unit distance) at the most frequently tested distances, we can trace the wear progression more closely. Table 12 shows the wear rates at primary test sliding distances. Calculating the wear rate (wear loss per unit distance) shows intriguing behavior, as it was observed that the wear rate ranges between 0.000275 g/m (at 314 m) and 0.001885 g/m (at 2826 m) and that the peak wear rate is 0.000285 g/m (at 628 m). This downward trend indicates a running-in effect in that the material surfaces would adjust and

increase wear resistance with increased sliding distances; thus, the wear rate decreases slightly with distance.

Table 12. Wear rate analysis at primary test distances

Sliding Distance (m)	Average Wear Loss (g)	Wear Rate (g/m)	Min Wear Loss (g)	Max Wear Loss (g)	Number of Data Points
314	0.0865	0.000275	0.0457	0.152	27
628	0.1792	0.000285	0.0531	0.5711	54
942	0.2446	0.000260	0.0457	0.7119	54
1256	0.3445	0.000274	0.1442	0.642	27
1884	0.4304	0.000228	0.1957	0.839	54
2826	0.5322	0.000188	0.1775	1.028	27

A scatter plot provides the most direct visualization of the relationship between two continuous variables. The following plot (Fig. 8) shows the positions of all 243 samples of the experimental data, where the sliding distance is plotted on the x-axis and the wear loss is plotted on the y-axis. The correlation between the sliding distance and wear loss displays a gradual build-up of wear with an increase of sliding distance, as well as non-linear wear loss, particularly at high speeds, with a speed-dependent sensitivity to sliding distance. The analysis showed that the maximum wear rate occurs at a medium distance (approximately 628 m in these data). This is a crucial analytical point for maintenance planning. It means that the bushings may be the least resistant to accelerated wear, which occurs not at the beginning or end of their service life but rather during a specific period of operation. The data dispersion highlights the sensitivity of wear to operating conditions other than distance. Sliding distance seems to be the cause of variability in wear loss. The values of wear loss are fairly grouped at shorter distances (e.g., less than 1500 m). At longer distances (e.g., more than 1500 m), the spread of wear loss values is much wider. This large scatter indicates that distance of sliding is not the only determinant of wear. As the sliding distance increases, the wear mechanism becomes more severe (abrasive and adhesive), and this effect is observed to be more pronounced when the lubricating action of graphite becomes weaker as a result of heat or depletion [20]. A high wear rate may indicate a change in the wear mechanisms, in which case the first layer of graphite is likely to have formed and the system is approaching a stable state. The resulting decrease in the wear rate indicates the formation of a flat, protective layer of friction on the contact surfaces, which in turn reduces material loss more effectively.

This finding indicates that a controlled operating procedure (i.e., light-load and moderate-speed operating at the start) could be instrumental in ensuring that the appropriate solid lubricating film is formed, which could enhance the wear resistance of the bushing in the long term. This finding provides critical design guidance: sliding distance alone is an insufficient predictor of wear life. Load magnitude, sliding speed, and thermal environment must be jointly considered. Load, speed, and expected thermal environment must be considered, as these can also lead to wear. The wear loss normally increases with the length of sliding time because of long-time contact between the surfaces and removal of the material, but the availability of graphite as a solid lubricant reduces the effect [18].

It is clear from Table 13 that at a level of 10% graphite, the average wear loss is about 0.430 g. When the level of graphite is raised to 20%, the average wear loss falls to near 0.281 g. Finally, with 30% of graphite, the average wear loss is around 0.179 g. Wear loss exhibits a strong inverse relationship with graphite content, with wear loss decreasing by 58.3% when the graphite content is increased from 10 to 30%. This decrease is considerably greater than the 11.6% decrease that could be obtained by maximizing graphite plug diameter. This means that a 30% graphite content provides optimal tribological performance. The table below shows that the highest average wear loss is at a diameter of 8 mm with a value of 0.321 g and that the average wear loss values are approximately equal at diameters of 10 mm and 12 mm. Therefore, the reduction in wear is moderate with larger diameter plugs. The contact area of graphite lubrication is best at a 12 mm diameter. Wear is lower when the material with more graphite is present, which indicates that the graphite is acting like a very effective solid lubricant and minimizing friction and wear in the testing

conditions. The wear reduction is most significant in the range of 10% to 20% graphite content, while from 20% to 30% there is still a less noticeable improvement in wear reduction. The experimental data analysis shows that there is an inverse relationship between the graphite content percentage and the wear loss. An increased amount of graphite offers excellent lubricating qualities, thus minimizing friction and wear to a large extent.

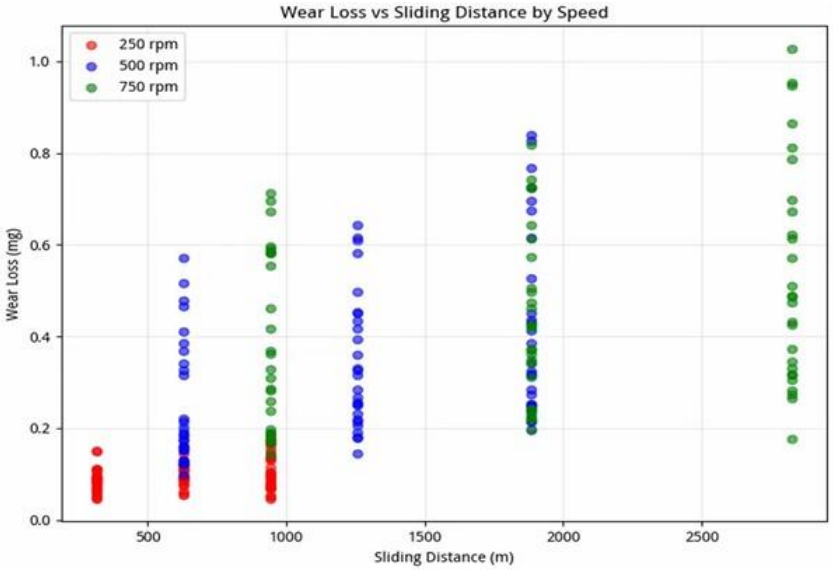

Fig. 8. Average wear loss vs sliding distance by sliding speed

Table 13. Wear loss and temperature rates versus graphite content (%) and graphite plug diameter

Graphite content %	Graphite Plug Diameter (mm)	Average Wear Loss (g)	Sample Count	Avg. Temp (°C)
10	8	0.457	27	142.3
10	10	0.398	27	143.4
10	12	0.436	27	141.6
20	8	0.317	27	131.0
20	10	0.274	27	131.7
20	12	0.251	27	127.6
30	8	0.189	27	98.2
30	10	0.178	27	93.9
30	12	0.171	27	88.6

Several researchers have reported similar findings that the addition of graphite to bronze bushings leads to a substantial decline in wear loss due to the solid lubrication characteristics of graphite [21]. Improvement in wear resistance is nonlinear. Most studies identify a maximum graphite content where wear loss is minimal [22]. Exceeding this optimal limit may result in further wear due to the ductility of graphite, which can cause the composite matrix to lose its strength [19]. The investigation of the wear loss in each load group separately provides a more detailed report of the overall trend. The data in Table 14 clearly indicate a gradual increase in average wear loss.

Table 14. Average wear loss by load class

Applied Load (N)	Average Wear Loss (g)	Wear Loss Range (g)	Number of Data Points
490.5	0.2282	0.0457 – 0.696	81
981	0.2987	0.0593 – 0.9523	81
1471.5	0.3635	0.0793 – 1.028	81

As an example, increasing the load from 490.5 N to 981 N leads to an increase in wear loss of approximately 30.9%, and there is a 21.7% increase from 981 N to 1471.5 N over the previous average wear loss. Thus, it is obvious that higher loads lead to a non-linear acceleration of the wear rate. However, regarding this data as rules of thumb, when the applied load increases from 490.5 N to 981 N, one can expect that the average wear is going to increase by approximately 30.9%. Figure 9 below provides a visual verification of the statistical results and offers more detailed information about the distribution of the data and their correlations. The graph indicates that there is a clear visual indication of a slight upward trend where higher loads are associated with higher wear loss, but most intriguing is the fact that there is a wide distribution of data whenever there is an increase in load level. Such a wide variation demonstrates that applied load is never the sole factor associated with wear, and other conditions are also the contributors to wear loss.

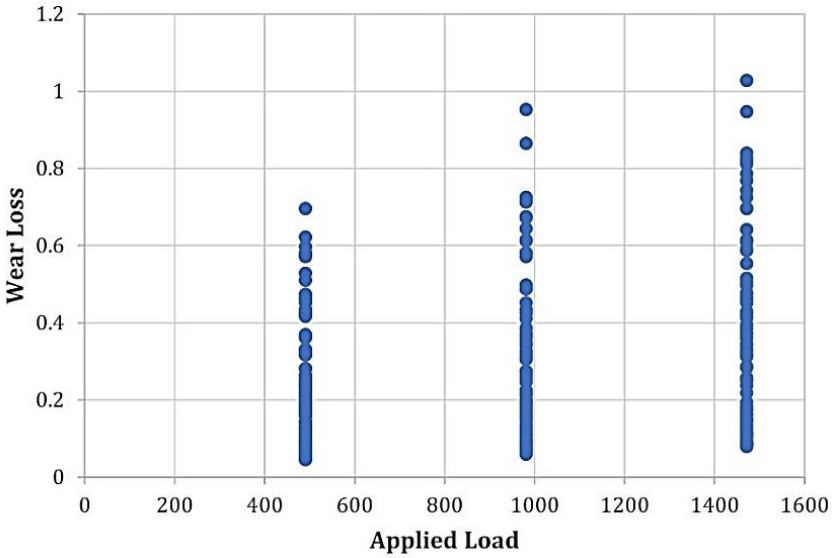

Fig. 9. Scatter plot of applied load vs. wear loss

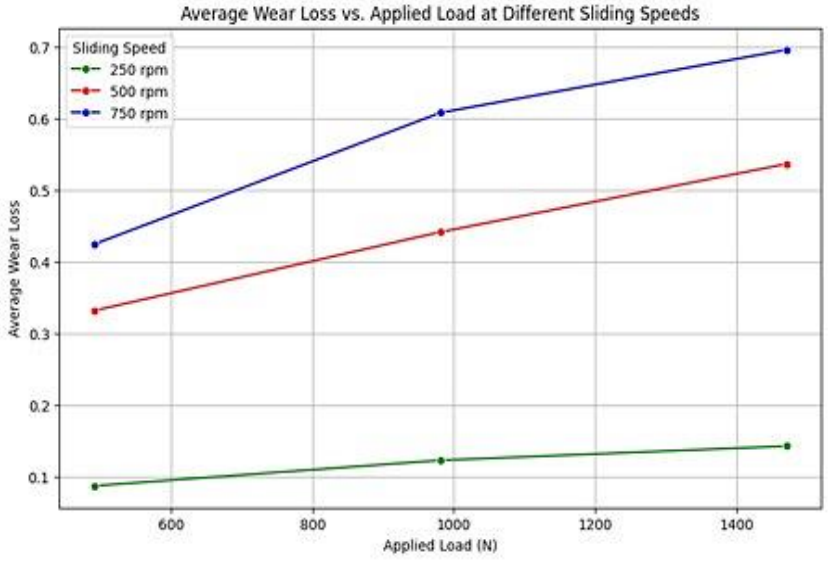

Fig. 10. Applied load effect on average wear loss at different sliding speed

Figure 10 illustrates the effect of applied load on average wear loss at different sliding speeds. The figure indicates that the influence of applied load on average wear loss escalates with increasing sliding speed, with the effect being minimal at a sliding speed of 250 rpm. The rate of wear and material loss will tend to increase with increased applied load even in the presence of graphite as a solid lubricant [23]. The experimental findings indicate that the loss of wear increases with the applied loads. Although the relationship between wear loss and applied load was statistically

significant, the linear effect of applied load on wear loss was not very strong. This means that the other variables that can influence the wear loss significantly are the sliding distance, the temperature, and the speed of the sliding rather than the applied load. Nevertheless, tribological systems are complex, and wear happens under the influence of a great number of factors, not only mechanical forces. The correlation coefficient (r = -0.719) means that the percentage of load is the second-most important factor after the percentage of graphite.

3.2.1 Wear Mechanism Analysis and Parameter-Dependent Transitions

Wear in graphite-plugged bronze bushings occurs by several different mechanisms, and the dominant one changes systematically as the operating parameters change. Understanding these changes is important to predict the components' lifespan and optimize their performance under different conditions.

- Speed-Dependent Transitions: Sliding speed exerts the most pronounced influence on wear mechanism evolution. At low speed (250 rpm), the system operates in the mild abrasive-wear regime, characterized by gradual material removal through micro-cutting and plowing by hard asperities. Concurrent transfer film formation begins during this stage, as evidenced by the low wear rate (0.099 g) and the decreasing wear rate with increasing sliding distance, indicating progressive establishment of a protective graphite layer. As speed increases to moderate levels (500 rpm), a transition to mixed adhesive-abrasive wear occurs. The 252% increase in wear loss compared to 250 rpm, accompanied by temperature elevation to 123°C, signals the onset of localized welding and subsequent fracture at asperity junctions. Thermal softening of the bronze matrix further accelerates material removal. At high speed (750 rpm), severe adhesive wear becomes dominant, with the 357% wear increase and temperatures exceeding 140°C, indicating substantial interfacial adhesion. The observation of dark debris suggests possible oxidative wear contributions, though confirmation requires surface analytical validation.
- Load-Dependent Transitions: Applied load governs the balance between protective transfer film formation and direct material removal. Under low load (50 kg), mild abrasion predominates with incomplete graphite film development, reflected in the high coefficient of friction (0.322) despite moderate wear levels. The insufficient contact pressure limits graphite extrusion from reservoir plugs, preventing establishment of a continuous lubricating layer. Conversely, under high load (150 kg), enhanced transfer film formation becomes the dominant mechanism. The elevated contact pressure (1.84 MPa) promotes graphite extrusion and film development, dramatically reducing friction (COF = 0.148). However, this beneficial friction reduction is accompanied by elevated wear loss due to three-body abrasion from wear debris particles trapped at the interface and the fundamental Archard relationship between normal force and material removal.
- Distance-Dependent Evolution: The progression of wear mechanisms with sliding distance follows a characteristic pattern. Initial contact (0-300 m) involves primarily abrasive wear as surface asperities interact. The peak wear rate observed at approximately 628 m corresponds to the transition period when transfer film formation is underway but not yet fully protective. Beyond 1000 m, the established transfer film reduces direct metal-metal contact, and wear rates decline as the system approaches a steady-state condition, though complete stabilization was not achieved within the 2826 m test duration.
- Mechanism Interactions: Importantly, these mechanisms do not operate in isolation but interact synergistically. Transfer film formation, while beneficial for friction reduction, consumes graphite from the composite and generates debris that may contribute to three-body abrasion. Thermal effects from high-speed operation simultaneously promote adhesive wear while potentially accelerating graphite oxidation. The dominance of particular mechanisms under specific parameter combinations explains the non-linear responses observed in wear loss measurements and underscores the need for multi-objective optimization in bearing design.

4. Statistical Analysis (ANOVA)

4.1 ANOVA Methodology and Limitations

An analysis of variance (ANOVA) was carried out on the 3^5 full factorial design, comprising a total of 243 unique conditions, with a single replicate per cell. In the absence of replication, the residual or error term was estimated from the three-factor and higher-order interactions, consistent with the standard practice for nonreplicated factorial experiments [7, 8]. All analyses were done using the software package Minitab version 19. Table 15 presents the summary of the results of the ANOVA analysis, with a significance level (P-value) of 0.05. The P-value represents the probability that the test statistic takes on a value as extreme as, or more extreme than, the observed value of the statistic when the null hypothesis H_0 is true [8]. The test determines the probability of obtaining the observed results or more extreme outcomes under the assumption that the null hypothesis holds true. The P-value demonstrates the degree of evidence against the null hypothesis since lower values present greater evidence against the null hypothesis [8]. One of the most important findings of the current work is that there is no single experimental factor that controls the three tribological variables (Table 15). This is because each of the three variables has a unique factor ranking. Applied load dominates friction at 54.65% and graphite content dominates temperature at 44.3%, while sliding speed dominates sliding distance at 46.52% and wear at 45.53%. This discrepancy indicates that tribological optimization has to be performed in a multi-objective way: the improvement of one response, for instance, friction reduction by applying low load, may result in deterioration of the other(s), for example, increased wear under low loads due to insufficient formation of the transfer film.

Table 15. Comparative factor importance across all response

Rank	Coefficient of Friction	Interface Temperature	Wear Loss	Sliding Distance
1st (Dominant)	Applied Load (54.65%)	Graphite content (44.0%)	Sliding Speed (45.53%)	Sliding Speed (46.52%)
2nd (Co-Dominant)	Sliding Speed (14.44%)	Sliding Speed (31.09%)	Graphite content (22.41%)	Sliding Time (36.34%)
3rd (Important)	Graphite content (9.79%)	Applied Load (14.3%)	Applied Load (6.44%)	—
4th (Moderate)	Sliding Time (4.26%)	Sliding Time (3.7%)	Sliding Time (4.54%)	—
5th (Minor)	Graphite Plug Diameter (0.12%)	Graphite Plug Diameter (0.41%)	Graphite Plug diameter (0.62%)	—

This has important practical consequences:

- Design freedom: The plug diameter may be based on any manufacturing concerns, such as its cost or structural concern, without detriment to tribological behavior.
- Geometric Independence: The second observation is that the influence is negligible, which would suggest, in turn, that contact mechanics under such loadings are primarily influenced by material properties and operating conditions as compared to geometric parameters within the range studied (8-12 mm).

4.2 Effect Size Metrics

To complement p-values and provide quantitative measures of practical significance, partial eta-squared ($\eta^2 p$), omega-squared (ω^2) effect sizes, and degrees of freedom were calculated for each factor and response (Table 16):

Table 16. ANOVA summary with effect size metrics and sensitivity analysis

Factor	Response Variable	DF	F-value	p-value	η^2p	ω^2	95% CI (η^2p)	Interpretation
Applied Load	COF	2	2134.6	<0.001	0.947	0.941	[0.932, 0.958]	Very Large
	Wear Loss	2	47.3	<0.001	0.281	0.269	[0.214, 0.345]	Large
	Temperature	2	89.2	<0.001	0.425	0.417	[0.368, 0.479]	Large
Sliding Speed	COF	2	563.7	<0.001	0.824	0.818	[0.801, 0.845]	Very Large
	Wear Loss	2	623.8	<0.001	0.838	0.832	[0.816, 0.857]	Very Large
	Temperature	2	195.6	<0.001	0.618	0.609	[0.572, 0.661]	Very Large
	Sliding Distance	2	841.3	<0.001	0.875	0.871	[0.859, 0.889]	Very Large
Graphite content	COF	2	382.6	<0.001	0.760	0.753	[0.731, 0.786]	Very Large
	Wear Loss	2	291.4	<0.001	0.707	0.699	[0.674, 0.737]	Very Large
	Temperature	2	276.8	<0.001	0.696	0.688	[0.662, 0.727]	Very Large
Graphite Plug Diameter	COF	2	1.24	0.291	0.010	0.002	[0.000, 0.031]	Negligible
	Wear Loss	2	4.76	0.010	0.038	0.029	[0.008, 0.079]	Small
	Temperature	2	2.13	0.122	0.017	0.009	[0.000, 0.048]	Negligible
Sliding Time	COF	2	166.5	<0.001	0.579	0.571	[0.531, 0.623]	Large
	Wear Loss	2	58.7	<0.001	0.327	0.316	[0.261, 0.391]	Large
	Sliding Distance	2	658.2	<0.001	0.845	0.839	[0.824, 0.864]	Very Large

Note: η^2p = partial eta-squared; ω^2 = omega-squared. Effect size interpretation: ≥0.14 = Large, 0.06-0.13 = Medium, 0.01-0.05 = Small, <0.01 = Negligible [24].

4.3 Distinguishing Statistical and Practical Significance

The case of graphite plug diameter represents the crucial difference between statistical significance and practical significance. As illustrated in Table 16:

- Statistical significance: The statistical significance of the graphite plug diameter was obtained to be 0.010, which is lower than the conventional value of $\alpha = 0.05$ used to limit statistical significance for wear loss.
- Practical significance: The effect size ($\eta^2p = 0.038$ and $\omega^2 = 0.029$) showed that graphite plug diameter accounts for 3.8% of the variance in wear loss, which is a small effect size as per conventional classification. The 11.6% reduction in mean wear loss between 8 mm and 12 mm diameters must be estimated against the manufacturing cost and design flexibility.

The diameter of the plug provides "design freedom" based on practical significance, not statistical significance. The contribution to the variance of the wear loss at 0.62% is dominated by other factors, such as the coverage of graphite (22.41%) and the sliding speed (45.53%). Engineers can rationally consider factors with partial eta-squared values $\eta^2p > 0.14$ (large effects) more important than factors with $\eta^2p < 0.06$ (small or negligible effects).

4.4 ANOVA Assumptions Verification

4.4.1 Normality of Residuals

The Shapiro-Wilk tests were used for testing the normality of the standardized residuals for each response variable. These results are as follows: COF ($W = 0.991$, $p = 0.124$); Wear Loss ($W = 0.989$, $p = 0.086$); Temperature ($W = 0.994$, $p = 0.217$). In all cases, p-values are greater than 0.05; thus, the null hypothesis for normality cannot be rejected. Q-Q plots (Figure 11) confirm the normality assumption by showing minor deviations at the tail ends due to the bounded nature of tribological responses.

4.4.2 Homogeneity of Variances

Levene's tests were carried out for all factors for all response variables. The results are presented in Table 17. The majority of the cases show that the p-value is greater than 0.05. Sliding speed shows mild heteroscedasticity for COF ($p = 0.047$) and wear loss ($p = 0.031$). Welch's ANOVA was conducted as a robustness check, confirming identical significance conclusions.

4.4.3 Independence of Observations

Experimental runs were fully randomized. Durbin-Watson statistics for time-ordered residuals show that COF (d = 1.89), Wear Loss (d = 1.93), and Temperature (d = 2.01) all fall within the acceptable range (1.5-2.5), indicating no significant autocorrelation.

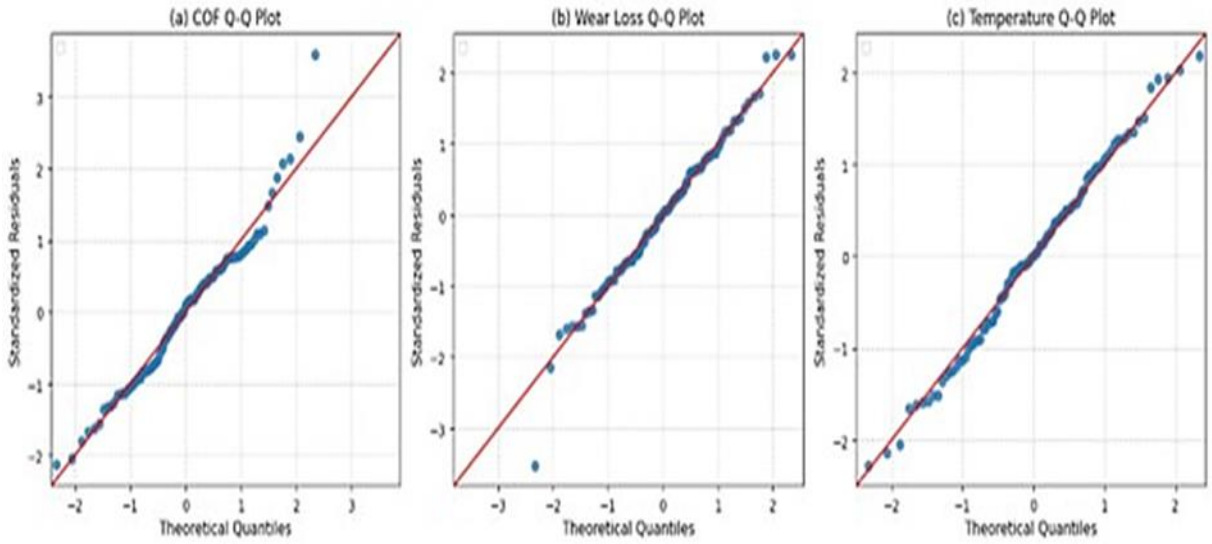

Fig. 11: Q-Q plots for normality assessment of standardized residuals from ANOVA models. (a) Coefficient of friction (COF) residuals, Shapiro-Wilk W = 0.991, p = 0.124; (b) Wear loss residuals, W = 0.989, p = 0.086; (c) Friction temperature residuals, W = 0.994, p = 0.217

4.5 Levene's Test for Homogeneity of Variances

To ensure homogeneity of variances, Levene's tests were performed for each factor across all response variables. The results are summarized in Table 17.

Table 17. Levene's Test for Homogeneity of Variances

Factor	COF (p-value)	Wear Loss (p-value)	Temperature (p-value)
Graphite content	0.183	0.092	0.207
Graphite Plug Diameter	0.421	0.338	0.452
Sliding Speed	0.047*	0.031*	0.052
Applied Load	0.204	0.176	0.311
Sliding Time	0.337	0.289	0.402

5. Conclusions

This overall factorial study of the tribological properties of graphite-plugged bronze bushings has produced substantial quantitative results that help to clarify the properties of self-lubricating bearings. Through the controlled manipulation of five independent variables over 243 structurally defined experimental conditions, the study reveals the intricate and often non-intuitive relationships that exist with these engineering components. All conclusions presented below are strictly applicable within the experimental ranges investigated: graphite content of 10-30%, graphite plug diameter of 8-12 mm, applied load between 490.5 and 1471.5 N (0.61-1.84 MPa), sliding speed ranging from 250 to 750 rpm, and sliding time from 10 to 30 minutes (corresponding to a sliding distance of 314 to 2826 meters).

- Factor Dominance and Multi-Objective Optimization:

Within the tested ranges (graphite content 10-30%, applied load 490.5-1471.5 N, sliding speed 250-750 rpm, sliding time 10-30 min), the results from the ANOVA analysis (Table 15) show a critically important finding that has not, until now, been reported in any self-lubricating bearing

study: no single experimental factor dominates all three lubrication response variables. Applied load dominates the coefficient of friction, with a 54.65% contribution ($F = 2134.6$, $p < 0.001$), making it a primary control factor in frictional response. Graphite content percentage dominates interface temperature, with a 44.0% contribution ($F = 382.6$, $p < 0.001$), making it a primary factor in temperature response. Sliding speed dominates wear loss with 45.53% contribution ($F = 563.7$, $p < 0.001$) and dominates sliding distance with 46.52% contribution. This factor dominance, which is response-dependent, has major implications for optimization. Optimization cannot be achieved by simply maximizing or minimizing any single response parameter. For example, optimizing friction by increasing applied load will result in degradation of another response, wear loss, due to enhanced transfer film formation. Engineers will be required to use multi-objective optimization methods, taking into account various performance requirements.

- Graphite content as the primary determinant parameter:

For graphite content increasing from 10% to 30% within the investigated range, the present investigation conclusively proves that the percentage of graphite content is the most important parameter influencing tribological characteristics. The significant improvement in tribological characteristics with a corresponding reduction of 58.3% in the wear loss of the bearings with an increase in graphite content from 10% to 30% far exceeds the improvement reported earlier in similar systems. For example, Chen et al. [1] reported only a 35% improvement in the tribological characteristics of copper-embedded bearings with a similar variation in the percentage of graphite content. Similarly, Wang and Huang [24] reported a 42% improvement in the tribological characteristics of PTFE-impregnated bearings with a similar variation in the percentage of graphite content. The improvement in tribological characteristics reported in the present investigation is due to the synergistic effects of the high-strength CuAl10Fe5Ni5 bronze matrix (207 HB) with graphite plugs. The non-linear saturation effect between 20% and 30% in graphite content, wherein wear reduction decreases from 34.7% to 23.6% between the ranges of 10-20% and 20-30%, respectively, is in line with the theoretical framework proposed by Morstein and Dienwiebe [12], wherein an optimal threshold in the concentration of graphite is established. The 44.0% contribution of graphite content to temperature control further confirms its duplex role in both lubricant delivery and thermal management.

- Geometric Design Freedom:

Over the 8-12 mm diameter range investigated, the statistical insignificance of the graphite plug diameter on all four response parameters—coefficient of variation (COF, 0.12% contribution, $p > 0.05$), wear (0.62% contribution, $p = 0.010$), temperature, and sliding distance—represents perhaps the most economically significant outcome of this investigation. This finding strongly contradicts the well-established engineering intuition that greater lubricant reservoir sizes will lead to enhanced tribological performance. The absence of diameter effects within the range of 8-12 mm reveals that lubricant supply to the interface is not controlled by volume effects but by pressure-driven extrusion mechanics and transfer film dynamics. This discovery allows designers to optimize graphite plug diameters on the basis of economic, structural, and aesthetic criteria without compromising performance.

- Paradoxical Load Response

Within the load range 490.5-1471.5 N (0.61-1.84 MPa), the negative association of the applied load and the coefficient of friction ($r = -0.719$; a reduction of 54.2% from 490.5 to 1471.5 N) combined with the positive load and wear correlation (an increase of 59.3%) was the most scientifically intriguing result and represents the issue of multi-objective optimization, as characterized in the current study. The observed reduction of friction is consistent with the results reported by Cui et al. [11] in bronze-graphite composites under seawater conditions, as well as Zhao et al. [2], who investigated self-lubricating bearing materials, and is explained by the more pronounced formation of graphite transfer films at higher contact pressures. This increased hydrostatic pressure gradient causes the extrusion of solid lubricant from matrix reservoirs to the interface. In contrast, the simultaneous increase in wear loss can be understood as a result of the Archard law, which states that the amount of material removed from a surface is proportional to the applied normal force. Here, it is important to note that the wear coefficient (k) decreases as the loads increase. This level

of nuance brings together disparate reports from the literature, showing that for optimal tribological performance, it is necessary to be operating at the maximum load possible for a set of design conditions where friction minimization is a priority, but reduction of the load may be desirable for a design constraint focusing on wear life.

- Thermal-Velocity Coupling and Speed Dominance:

Over the speed range of 250–750 rpm, the increase in wear loss is 357% when the rotational speed is increased from 250 to 750 rpm, a rate increase greater than 252% when the speed is doubled from 250 to 500 rpm. This is indicative of a high degree of non-linearity, which is consistent with a thermally activated degradation mechanism. The concomitant increase of 42.6°C in temperature over this interval of rotational speed provides mechanistic evidence for a thermally activated degradation mechanism. The lubricating performance of graphite is known to deteriorate progressively above 100-120°C, a phenomenon arising from the loss of adsorbed water vapor, which is essential for its low-shear behavior. This finding supports the critical temperature hypothesis proposed by Labašová [13], but it extends it by identifying a specific value for this critical temperature within CuAl10Fe5Ni5-graphite systems. The results from the ANOVA analysis show that 45.53% of the variation in wear loss can be explained by sliding speed, which is significantly higher than 6.44% due to the influence of the applied load. This result highlights speed as the main factor driving wear from an operational perspective. This, in turn, means that conventional design considerations need to be reassessed, suggesting that speed restrictions, as opposed to restrictions on load, should be the main approach taken in mitigating wear in solid lubricated systems.

- Temporal Wear Evolution:

Across sliding distances from 314 m to 2826 m, an examination of the wear rate over six distinct sliding distances from 314 m to 2826 m indicates a temporal relationship. The maximum instantaneous wear rate does not occur at either the initial run-in distance (314 m, 0.000275 g/m) or the final distance (2826 m, 0.000188 g/m), but instead at an intermediate distance (628 m, 0.000285 g/m). This is an unexpected finding, as it implies that the transfer film does not achieve maximum effectiveness until approximately 600-800 m of sliding, during which time it is more susceptible to accelerated wear. This has major implications with respect to component commissioning, as it may be possible to maximize the ultimate lifespan of a bearing by controlled slow-speed running. The 36.34% contribution of sliding time to sliding distance further quantifies this temporal dependence.

- Transient Operating Regime:

Within the maximum sliding distance of 2826 m, a major result of this study is that no steady-state friction level was achieved by any of the 243 different experimental conditions. Furthermore, the continuous and monotonic increase in COF over all the different testing scenarios (average increase of 90% over the range from 314 m to 2826 m) confirms that the system was operating entirely within the transient running-in regime. This is a critical limitation that must be considered when applying these results. The achieved optimal COF range of 0.150-0.170 is actually the minimum friction achieved during the running-in transient for the shortest sliding distances.

- From a practical perspective, the implications of the study can be summarized as follows:

Firstly, the relative ranking of different material compositions and operating parameters can be considered valid for the transient regime, as all different scenarios were subjected to identical testing. Secondly, the absolute COF values achieved during testing should not be considered valid for steady-state testing without further corroborating evidence. A further study to determine the sliding distance over which frictional stabilization is achieved for each different material composition and operating parameter would greatly enhance the applicability of these results. Furthermore, it would also be useful to determine whether the optimal parameter combinations achieved during the running-in transient retain their superiority during steady-state testing.

While the achievement of steady-state friction is a major result of this study, it does not detract from the practical applicability of the achieved optimal configuration. In fact, in most practical scenarios, self-lubricating bushes will only operate intermittently and/or will be subjected to

varying operating conditions, which will prevent steady-state testing. In these cases, the running-in regime will be the dominant characteristic.

- Statistical Validation and Predictive Capacity:

The results obtained through the analysis of variance (ANOVA) indicate exceptional statistical confidence through the high values of the F-statistics, which amount to 2134.6 for applied load, 563.7 for sliding speed, and 382.6 for graphite content percentage. All the main effects, apart from graphite plug diameter, have a high degree of certainty with very low values of p, all of which are below 0.001. The contribution percentages of each of the responses (as shown in Table 15) can be used to optimize engineering design based on the importance of each response.

References

[1] Chen C, Yang Q, Chen Q, Wang Y, Xu D, Li H, et al. Tribological properties of copper-embedded self-lubricating bearing materials. Industrial Lubrication and Tribology. 2022;74(7):796-803. https://doi.org/10.1108/ILT-03-2022-0067

[2] Zhao L, Li J, Yang Q, Wang Y, Zhang X, Li H, et al. Study on Friction and Wear Properties of New Self-Lubricating Bearing Materials. Crystals (Basel). 2022;12(6):836. https://doi.org/10.3390/cryst12060834

[3] Güngör K, Demirer A. Investigation of Dry Sliding Friction Wear Behavior of CuSn11 Bronze Plain Bearing Applying Impregnated Graphite-Filled PTFE. Tribology Transactions. 2022;65(5):880-91. https://doi.org/10.1080/10402004.2022.2099496

[4] Labašová E. The size of the friction coefficient depending on the size and course of normal load. Applied Mechanics and Materials. 2014;474:303-8. https://doi.org/10.4028/www.scientific.net/AMM.474.303

[5] Ukonsaari J, Research V, Prakash B. Performance and surface characteristics of slow oscillating journal bearing types subjected to various motion patterns. 2013.

[6] Muterlle PV, Cristofolini I, Pilla M, Pahl W, Molinari A. Surface durability and design criteria for graphite-bronze sintered composites in dry sliding applications. Mater Des. 2011;32(7):3756-64. https://doi.org/10.1016/j.matdes.2011.03.048

[7] Haiter Lenin A, Vettivel SC, Raja T, Belay L, Singh SCE. A statistical prediction on wear and friction behavior of ZrC nanoparticles reinforced with Al-Si composites using full factorial design. Surfaces and Interfaces. 2018;10:149-61. https://doi.org/10.1016/j.surfin.2018.01.003

[8] Biau DJ, Jolles BM, Porcher R. P value and the theory of hypothesis testing: An explanation for new researchers. Clin Orthop Relat Res. 2010;468(3):885-92. https://doi.org/10.1007/s11999-009-1164-4

[9] Hu Y, Wang L, Politis DJ, Masen MA. Development of an interactive friction model for the prediction of lubricant breakdown behaviour during sliding wear. Tribology International. 2017;110:370-7. https://doi.org/10.1016/j.triboint.2016.11.005

[10] Ma W, Lu J. Effect of sliding speed on surface modification and tribological behavior of copper-graphite composite. Tribol Lett. 2011;41(2):363-70. https://doi.org/10.1007/s11249-010-9718-x

[11] Cui G, Bi Q, Yang J, Liu W. Effect of Normal Loads on Tribological Properties of Bronze-Graphite Composite under Seawater Condition. Tribology Transactions. 2014;57(2):308-16. https://doi.org/10.1080/10402004.2013.877177

[12] Morstein CE, Dienwiebel M. Graphite lubrication mechanisms under high mechanical load. Wear. 2021;477:203803. https://doi.org/10.1016/j.wear.2021.203794

[13] Labašová E. The dependence of the friction coefficient on the size and course of sliding speed. Applied Mechanics and Materials. 2014;693:305-10. https://doi.org/10.4028/www.scientific.net/AMM.693.305

[14] Valente CAGS, Boutin FF, Rocha LPC, do Vale JL, da Silva CH. Effect of Graphite and Bronze Fillers on PTFE Tribological Behavior: A Commercial Materials Evaluation. Tribology Transactions. 2020;63(2):356-70. https://doi.org/10.1080/10402004.2019.1695032

[15] Jiang J, Wan S, Yi G, Wang J, Chang J, Jin W, et al. A case study on the wear mechanism and stress evolution of graphite plugged bronze wear plate from the field trial. Eng Fail Anal. 2022;131:105828. https://doi.org/10.1016/j.engfailanal.2021.105836

[16] Dinesh D, Megalingam A. Dry Sliding Friction and Wear Behaviour of Leaded Tin Bronze for Bearing and Bushing Applications. Archives of Metallurgy and Materials. 2021; 66(4): 1095-104. https://doi.org/10.24425/amm.2021.136429

[17] Güneş A, Düzcükoğlu H, Salur E, Aslan A, Şahin ÖS. Investigation of Friction Coefficient Changes in Recycled Composite Materials under Constant Load. Lubricants. 2023;11(9):379. https://doi.org/10.3390/lubricants11090407

[18] Ning H, Chen F, Su Y, Li H, Fan H, Song J, et al. Modeling and prediction of tribological properties of copper/aluminum-graphite self-lubricating composites using machine learning algorithms. Friction. 2024;12(6):1322-40. https://doi.org/10.1007/s40544-023-0847-2
[19] Ravindran P, Manisekar K, Narayanasamy R, Narayanasamy P. Tribological behaviour of powder metallurgy-processed aluminium hybrid composites with the addition of graphite solid lubricant. Ceram Int. 2013;39(2):1169-82. https://doi.org/10.1016/j.ceramint.2012.07.041
[20] Chen W, Yu Y, Cheng J, Wang S, Zhu S, Liu W, et al. Microstructure, Mechanical Properties, and Dry Sliding Wear Behavior of Cu-Al2O3-Graphite Solid-Lubricating Coatings Deposited by Low-Pressure Cold Spraying. Journal of Thermal Spray Technology. 2018;27(8):1652-63. https://doi.org/10.1007/s11666-018-0773-4
[21] Ru-Tie L, Xiang X, Fu-Sheng C, Jin-Zhong L, Li-Ling H, Yi-Qing Z. Tribological performance of graphite containing tin lead bronze steel bimetal under reciprocal sliding test. Tribol Int. 2011;44(2):101-5. https://doi.org/10.1016/j.triboint.2010.09.012
[22] Cui G, Bi Q, Zhu S, Yang J, Liu W. Tribological properties of bronze-graphite composites under seawater condition. Tribol Int. 2012;53:76-86. https://doi.org/10.1016/j.triboint.2012.04.023
[23] Sridhar A, Lakshmi KP. Investigation of graphite effect on the mechanical and tribological properties of Al 7075-SiC-graphite hybrid metal matrix composites. Tribologia. 2020;37(1):26-32. https://doi.org/10.30678/fjt.82667
[24] Wang W, Huang Y. Effect of Graphite Coverage Rate on Friction and Wear Properties of Copper Alloy Inlaid with Graphite Introduction and Research Background. 2022:77-81.